

Article

Monitoring Land Cover Change on a Rapidly Urbanizing Island Using Google Earth Engine

Lili Lin ^{1,2}, Zhenbang Hao ^{2,3}, Christopher J. Post ⁴, Elena A. Mikhailova ⁴, Kunyong Yu ^{2,3},
Liuqing Yang ^{1,2} and Jian Liu ^{1,2,3,*}

¹ Landscape Architecture College, Fujian Agriculture and Forestry University, Fuzhou 350002, Fujian, China; lilil@g.clemson.edu (L.L.); liuqingyang@fafu.edu.cn (L.Y.)

² University Key Lab for Geomatics Technology and Optimized Resources Utilization in Fujian Province, Fuzhou 350002, Fujian, China; zhenbanghao@fafu.edu.cn (Z.H.); yuyky@fafu.edu.cn (K.Y.)

³ Forest College, Fujian Agriculture and Forestry University, Fuzhou 350002, Fujian, China

⁴ Department of Forestry and Environmental Conservation, Clemson University, Clemson, SC 29634, USA; cpost@clemson.edu (C.J.P.); eleanam@clemson.edu (E.A.M.)

* Correspondence: fjliujian@fafu.edu.cn; Tel.: +86-86392212

Received: 2 September 2020; Accepted: 10 October 2020; Published: 20 October 2020



Abstract: Island ecosystems are particularly susceptible to climate change and human activities. The change of land use and land cover (LULC) has considerable impacts on island ecosystems, and there is a critical need for a free and open-source tool for detecting land cover fluctuations and spatial distribution. This study used Google Earth Engine (GEE) to explore land cover classification and the spatial pattern of major land cover change from 1990 to 2019 on Haitan Island, China. The land cover classification was performed using multiple spectral bands (RGB, NIR, SWIR), vegetation indices (NDVI, NDBI, MNDWI), and tasseled cap transformation of Landsat images based on the random forest supervised algorithm. The major land cover conversion processes (transfer to and from) between 1990 and 2019 were analyzed in detail for the years of 1990, 2000, 2007, and 2019, and the overall accuracies ranged from 88.43% to 91.08%, while the Kappa coefficients varied from 0.86 to 0.90. During 1990–2019, other land, cultivated land, sandy land, and water area decreased by 30.70%, 13.63%, 3.76%, and 0.95%, respectively, while forest and built-up land increased by 30.94% and 16.20% of the study area, respectively. The predominant land cover was other land (34.49%) and cultivated land (26.80%) in 1990, which transitioned to forest land (53.57%) and built-up land (23.07%) in 2019. Reforestation, cultivated land reduction, and built-up land expansion were the major land cover change processes on Haitan Island. The spatial pattern of forest, cultivated land, and built-up land change is mainly explained by the implementation of a ‘Grain for Green Project’ and ‘Comprehensive Pilot Zone’ policy on Haitan Island. Policy and human activities are the major drivers for land use change, including reforestation, population growth, and economic development. This study is unique because it demonstrates the use of GEE for continuous monitoring of the impact of reforestation efforts and urbanization in an island environment.

Keywords: anthropogenic activities; forest change; GEE; LULC; urbanization

1. Introduction

Islands consist of isolated land surrounded by water, making them particularly sensitive to environmental and anthropogenic changes. Climate change, overpopulation, and other human activities have considerable impacts on island ecosystems and the environment. Rapid island development and utilization can quickly cause irreversible damage to the environment [1]. Some rapidly developing islands are undergoing significant changes due to urbanization. Land cover change is a significant

indicator to help identify land-system dynamics and environmental development [2–4]. Therefore, mapping land cover change in a developing island is critical for supporting sustainable development and land-use policy-making.

Mapping of land cover change using satellite remote sensing data has been reported by many researchers [3,5]. For instance, Shifaw et al. (2019) [6] monitored farmland dynamics on Pingtan Island using ENVI software. Kuemmerle et al. (2016) [2] assessed the spatial patterns of land cover change using land cover change indicators. Abdullah et al. (2019) [4] used the advanced feature selection and classification techniques to assess multi-temporal land use and land change (LULC) changes. Viana et al. (2019) [7] proposed a novel method to classify long-term satellite images. These studies successfully tracked land cover over time and the main challenge for wider adoption is the requirement of computers with substantial processing capability and specialized software (e.g., ENVI, ArcGIS, ERDAS, etc.) to classify remote sensing images. These specialized software packages need significant computer resources and time to process multiple years of imagery over large spatial extents, and it is challenging to process remote sensing images because of the data size of the imagery.

In contrast to the traditional remote sensing processes, Google Earth Engine (GEE) has shown great potential for land cover classification [8]. It is a cloud computing platform for environmental monitoring and analysis (<https://earthengine.google.com/>) [9,10], which can handle big data processing rapidly [8]. In addition to various automatic mapping approaches, it also hosts a vast public data catalog, including a series of remote sensing data (e.g., Landsat images, MODIS), topography, land cover, weather, and population [10], which are updated as new data products become available. GEE provides multiple examples to support imagery classification, including filter image collection, simple cloud score, Landsat simple composite, and cloud masking. These examples help users to classify LULC more efficiently and easily. This platform has been used by researchers in numerous studies for forest change detection [11,12], habitat tracking [13], urban land mapping [14,15], and human activity [16], indicating that GEE is very useful in observation and environmental analysis. For instance, forest cover and change analysis has been performed in GEE, which helps to monitor and improve the sustainability of the regional environment. Tamiminia et al. (2020) [17] concluded that the most-used datasets in GEE are: vegetation indices (27%), Hansen global forest (17%), land cover (17%), and canopy height (5%), which are all related to forests. Besides estimating forest biophysical parameters, it is used to explore the forest change at global, national, and regional scales. Measuring trends in forest change have been reported in previous research, such as using the Normalized Difference Vegetation Index (NDVI) change to detect the land cover change [18–20] and Enhanced Vegetation Index (EVI) change to monitor land degradation and restoration [21]. However, few studies discuss the process and trends of LULC changes on a rapidly developing and urbanizing island.

In China, many cities have experienced unprecedented urbanization over the past three decades [4]. As the fifth-largest island in China, the main change of land cover that has occurred on Pingtan Island over the past 30 years is due to its strategic position on the southeast trade routes [22]. Pingtan Island has fragile ecosystems, which makes it prone to severe soil loss during heavy rainstorms and through wind erosion on the island [23]. With the implementation of China's reforestation strategy 'Grain for Green Project' [24,25], the first-phase construction of coastal shelter forests was carried out by the Fujian government from 1988 to 2000, followed by the second phase of coastal shelter forests planting between 2000 and 2005. Subsequently, China's policy to boost the economy and social development was initiated through a 'Comprehensive Pilot Zone' program that was started in Pingtan County in 2009, which led to accelerated development of the island. Next, in 2014, Pingtan Island was approved as a free trade zone [26]. It was also planned to be built into an international tourism island as well as an important regional economic hub. As a result, Pingtan Island has undergone substantial change in recent years, with the total gross domestic product (GDP) increased from 46.03 million USD to 4159.56 million USD (1990–2019). Notably, it has achieved substantial change in reforestation [25], which plays a highly critical role in protecting the Pingtan Island environment by blocking wind and stabilizing the soil. Although several studies have documented changes on this island, such as

coastline change [9] and tourism [10], few studies have examined the spatio-temporal patterns of land use change in this island environment.

This study leveraged GEE to map the LULC dynamics and major land cover conversion process on Haitan Island (the largest island of Pingtan County). Satellite images from 1990, 2000, 2007, and 2019 were chosen to capture the mostly undeveloped state in 1990, when the island had undergone reforestation in 2000, after reforestation and before the comprehensive development establishment in 2007, and 10 years after the initiation of ‘Comprehensive Pilot Zone’ development in 2019. The objectives of this study were to quantify the impacts of a national reforestation program through land cover conversion and analyze the driving factors for land use change.

2. Materials and Methods

2.1. Study Site

Haitan Island is the main island of Pingtan County, Fujian, China (Figure 1). It covers approximately 267 km² land area and is comprised of seven towns and four villages. The region is characterized by marine accumulation plains, with the highest elevation in Junshan mountain (434.40 m above the mean sea level). The plains are mainly located in the middle of the island, while mountains and hills are in the north and south. The soil here is poor and acidic (laterite soil: 46%, sandy soil: 23.35%) [27]. The area is dominated by marine monsoon climate, with a mean annual temperature of 19.6 °C and mean annual precipitation of 1000–1200 mm.

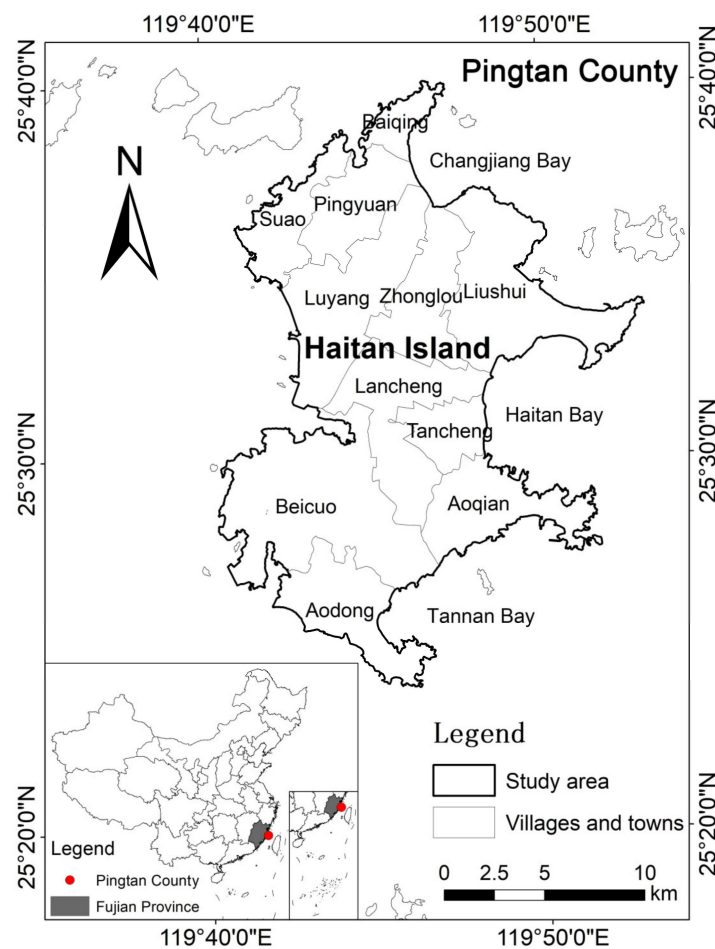


Figure 1. Location of the study site, Haitan Island, within Pingtan County, Fujian, China.

It has an extensive sandy coastline, including many beaches, such as Changjiang, Tannan, Longfengtou, and Haitan. Due to its geographic location, the residents' living environment is impacted by frequent strong winds, especially the prevailing north-northeast wind in the winter season [6,23,28]. Many reforestation measures have been implemented for the purpose of environmental protection [29]. The major planted forest types are beach sheoak (*Casuarina equisetifolia*), black pine (*Pinus thunbergii*), acacia (*Acacia confusa*), and slash pine (*Pinus elliottii*) [27].

2.2. Data Collection

The data processing flowchart for this study is presented in Figure 2. First, the cloudless composite Landsat images for 1990, 2000, 2007, and 2019 (Section 2.2.1) and the maximum value of NDVI [19] in the given year were calculated in GEE (Section 2.4). The administrative boundary, forest inventory data, and 1:10,000 topographic map of Pingtan County were obtained from Fujian Forestry Bureau, and socio-economic data were collected from Fuzhou Statistical Yearbook. Second, the classification and accuracy assessment (Section 2.3) were performed in GEE. Except for the field survey data as additional validation in 2007, other samples were all collected in Google Earth Pro by visual interpretation. Finally, the major land cover conversion between 1990 and 2019 was mapped to identify the spatial pattern and process, using maximum NDVI to understand the influence of LULC changes on Haitan Island.

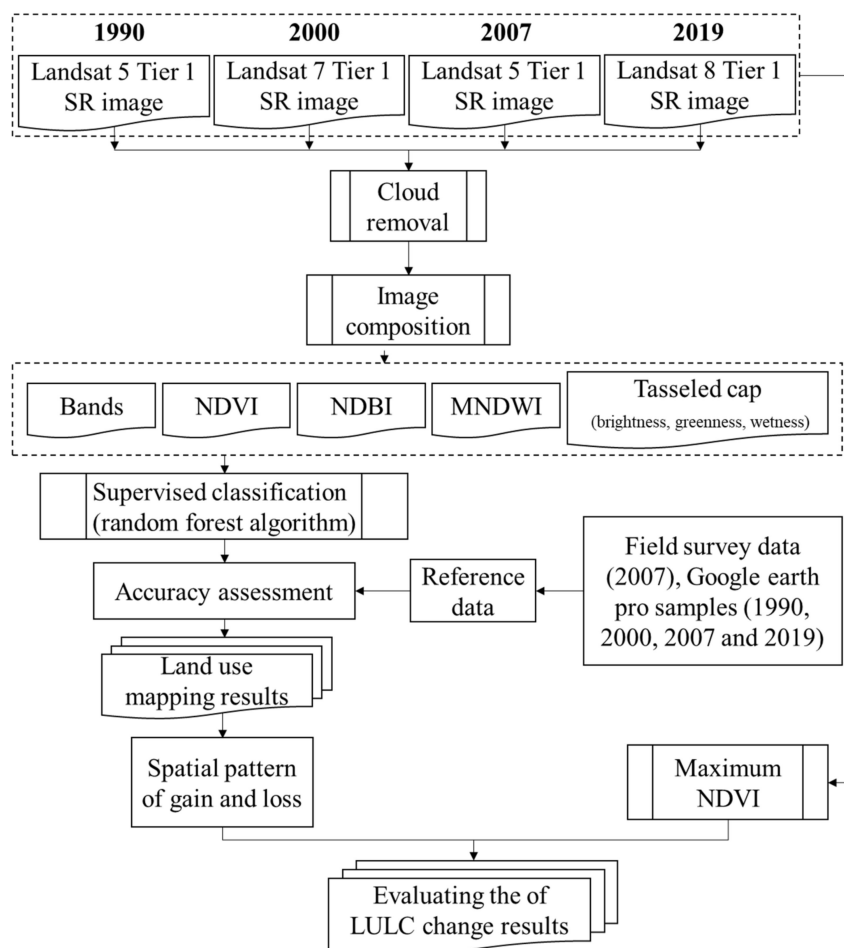


Figure 2. The flowchart of data processing in this study. SR = Surface reflectance; NDVI = Normalized Difference Vegetation Index; NDBI = Normalized Difference Built-up Index; MNDWI = Modified Normalized Difference Water Index; LULC = Land use and land cover.

2.2.1. Image Preprocessing

GEE provides a rapid analysis using Google's computing infrastructure, which offers online datasets in near-real time [10]. Landsat 5 Surface Reflectance images (1990, 2007), Landsat 7 Surface Reflectance images (2000), and Landsat 8 Surface Reflectance images (2019) were selected for Haitan Island land cover classification in GEE (Table 1).

Table 1. Data sources used in this study.

Data Layer	Source	Spatial Resolution (m)	Year
Landsat 5 Surface Reflectance	GEE dataset (USGS)	30	1990, 2007
Landsat 7 Surface Reflectance	GEE dataset (USGS)	30	2000
Landsat 8 Surface Reflectance	GEE dataset (USGS)	30	2019
Administrative boundary	Fujian Forestry Bureau	-	2003, 2016
Forest inventory data	Fujian Forestry Bureau	-	2003, 2016
1:10,000 topographic map	Fujian Forestry Bureau	1	-
Socio-economic data	Fuzhou Statistical Yearbook	-	1990–2019

Images were selected and mosaicked based on the quality assessment band flags to minimize the effects of clouds and clouds' shadows. Simultaneously, the spectral bands in Landsat image, including red, green, and blue bands (RGB), near-infrared (NIR), and short-wave infrared (SWIR), were selected for classification. In addition, NDVI [19], Normalized Difference Built-up Index (NDBI) [18], Modified Normalized Difference Water Index (MNDWI) [14,18], and tasseled cap transformation (brightness, greenness, wetness) [30,31] were calculated and added to the bands, which are helpful for land use classification [18,32]. All of the processing was conducted in GEE Code Editor (<https://code.earthengine.google.com/>).

2.2.2. Land Cover Classes

Land cover types were divided into six classes (sandy land, built-up land, cultivated land, forest land, other land, and water) in this study (Table 2) [27]. Next, the samples were selected from historical images in Google Earth Pro using a visual assessment. A total of 1000 sample points were collected in 1990, 2000, 2007, and 2019, respectively. The collected samples were divided into 70% training data and 30% validation data.

Table 2. The description of land cover classes on Haitan Island, China.

Land Cover Classes	Description
Sandy land (SL)	Beaches
Built-up land (BL)	Residential areas and other built-up land, such as roads, industrial land
Cultivated land (CL)	Cultivated, fallow farmland and terraced
Forest land (FL)	Forest, grassland, orchard, and urban greening land
Other land (OL)	Unused land or hard-to-use land, including rocks and bare soil
Water (W)	Rivers, reservoirs, lakes, dams and oceans

2.3. Image Classification and Accuracy Assessment

There are several classifier packages for supervised classification in GEE, such as Random Forests (RF), Classification and Regression Trees, Support Vector Machine, and Naïve Bayes [9]. Many researchers reported higher accuracy was achieved using RF classifier algorithm [18,33,34]. The RF algorithm is an ensemble learning method, which consists of many individual decision trees [5]. Each individual decision tree has several nodes, and the final result is determined by the majority vote. The advantage of RF is that it can produce a highly accurate classifier and handle thousands of input variables [35]. Thus, RF was used to obtain the classification maps in this study.

For the year of 2007, 114 field samples (with GPS locations) were collected in December of 2007, which were additional samples for validation. The field samples covered each type and were distributed as uniformly as possible in the accessible areas of Haitan Island. The GPS coordinate was collected three times in each sample, and the mean (X, Y coordinate) was taken as the location of sample. All the samples were unloaded in GEE. Since the early Google Earth satellite images (1990 and 2000) that cover Haitan Island were lower resolution than the image in the year 2019, topographic map and forest inventory data were used as auxiliary data to delineate the reference points. Finally, all the reference data was uploaded in GEE for accuracy assessment. According to the confusion matrix for each year in GEE, user's accuracy, producer's accuracy, overall accuracy, Kappa coefficient, and F1 score [18,36] were calculated to evaluate the classification results [9]. F1 score ranged from 0 to 1, which was calculated based on the combination of producer's and user's accuracy. The higher value of F1 score means higher accuracy achieved. Finally, the land use classified maps were downloaded from GEE.

2.4. Detection of Land Cover Change

The spatial patterns of land cover change are critical to understanding the LULC process and for helping policymakers adopt appropriate practices for the region's sustainable development. Thus, the gain and loss of major land cover types were calculated as follows (Equations (1)–(3)):

$$K_{\text{gain}} = S_b - S_a \quad (1)$$

$$K_0 = S_{b_i} = S_{a_i} \quad (2)$$

$$K_{\text{loss}} = S_a - K_0 \quad (3)$$

where S_a and S_b are the land cover type at the initial and end of time in a given period, respectively. S_{a_i} and S_{b_i} are the unchanged area of the same land cover type in the initial and end of time.

In addition, NDVI is useful for environmental monitoring, particularly in vegetation growth measurement (Equation (4)) [17,19,37]. Therefore, the maximum NDVI value composition was calculated from all the available images in the years of 1990, 2000, 2007, and 2019 to understand the influence of LULC changes in this study:

$$\text{NDVI} = (\text{NIR} - \text{Red}) / (\text{NIR} + \text{Red}) \quad (4)$$

where NIR and Red are the values of near-infrared and red band, respectively, in Landsat image.

3. Results

3.1. Land Cover Classification and Accuracy Assessments

The land cover classification maps of the years 1990, 2000, 2007, and 2019 are shown in Figure 3a–d, which were produced using random supervised classification. The RF classifier produced good overall accuracies for Haitan Island, with overall accuracy assessments of 90.09% (1990), 90.31% (2000), 91.08% (2007), and 88.43% (2019), respectively, and the Kappa accuracies were 0.88 (1990), 0.89 (2000), 0.90 (2007), and 0.86 (2019) (Table 3). For each class type, the user's accuracies and producer's accuracies ranged between 80–100% in each year. Water had high classification accuracies in each year because its reflectance is easier to distinguish from other categories, whereas sandy land and other land had low accuracies.

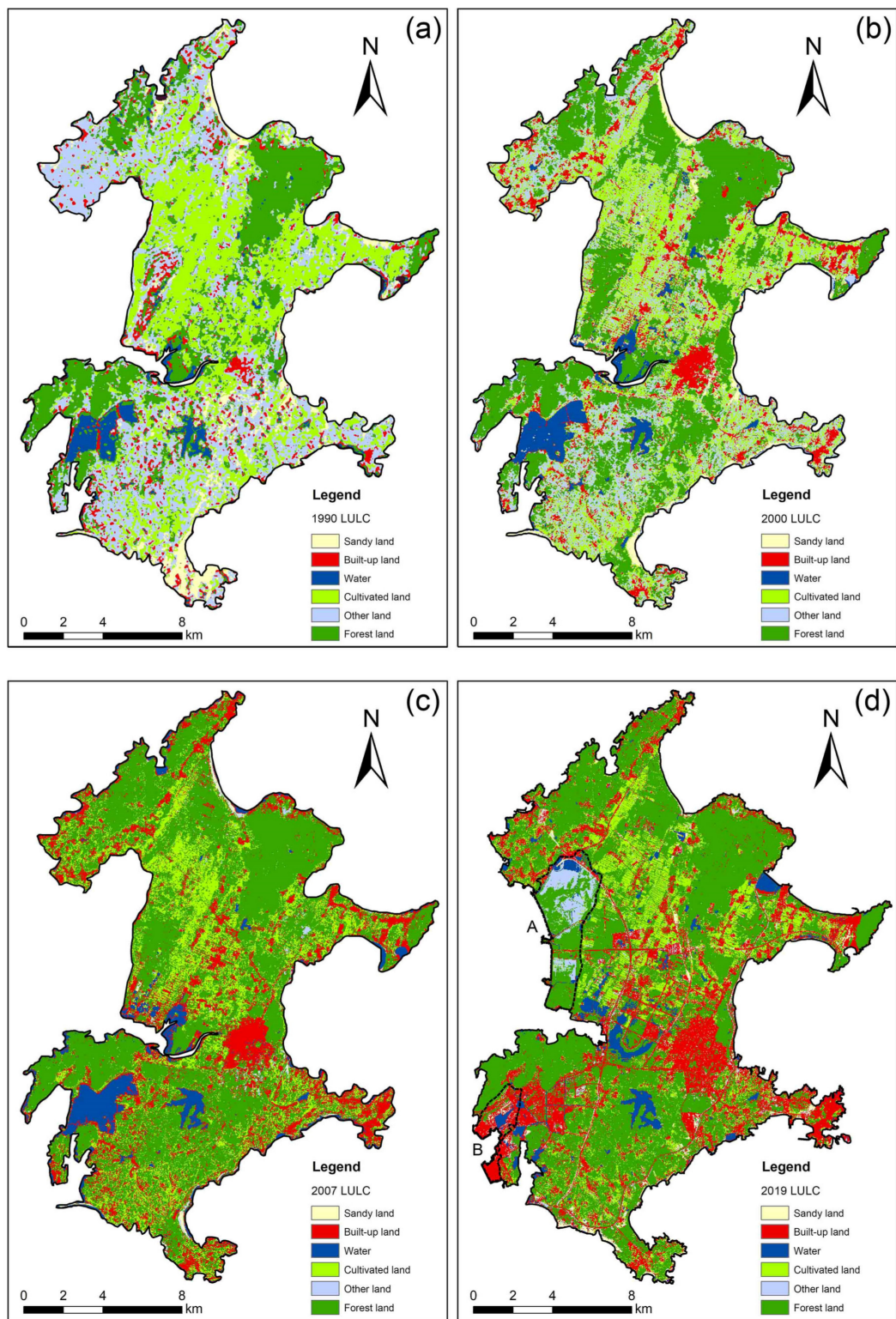


Figure 3. Land cover classification on Haitan Island: (a) 1990, (b) 2000, (c) 2007, and (d) 2019. A is the Xingfuyang area. A, B in (d) 2019 is the different area compared to 1990, 2000, and 2007, due to reclamation.

Table 3. User’s accuracy, producer’s accuracy, overall accuracy, and Kappa coefficient on Haitan Island, China, by land cover classes.

Accuracy Assessment	Land Cover Classes						Overall Accuracy	Kappa Coefficient
	SL	BL	CL	FL	OL	W		
Year: 1990								
User’s accuracy	83.33%	91.11%	86.05%	93.33%	88.10%	97.37%	90.09%	0.88
Producer’s accuracy	93.02%	91.11%	90.24%	85.71%	80.43%	100.00%		
F1 score	0.88	0.91	0.88	0.89	0.84	0.99		
Year: 2000								
User’s accuracy	82.98%	91.30%	88.37%	95.24%	88.64%	97.22%	90.31%	0.89
Producer’s accuracy	92.36%	89.36%	86.36%	88.89%	86.67%	100.00%		
F1 score	0.87	0.90	0.87	0.92	0.88	0.99		
Year: 2007								
User’s accuracy	82.61%	92.68%	87.18%	92.31%	88.10%	97.22%	91.08%	0.90
Producer’s accuracy	92.68%	90.48%	89.47%	90.57%	86.05%	97.22%		
F1 score	0.87	0.92	0.88	0.91	0.87	0.97		
Year: 2019								
User’s accuracy	83.97%	89.29%	84.41%	95.39%	82.61%	99.31%	88.43%	0.86
Producer’s accuracy	80.62%	88.03%	92.39%	85.29%	82.31%	99.65%		
F1 score	0.82	0.89	0.88	0.90	0.82	0.99		

NOTE: SL = sandy land, BL = built-up land, CL = cultivated land, FL = forest land, OL = other land, W = water.

3.2. The 30-Year Land Cover Change

Table 4 shows the land cover area and change of Haitan Island over the 30 years. The main trend of land cover type change is that forest area has increased by 92.36 km² of the study area, followed by other land categories declining by 79.05 km² of the study area, and expansion of built-up land by 47.27 km² of the study area. Compared to the final and initial period for each land cover type, the rate of land cover change of built-up land and forest land increased by 264.43%, and 156.85%, respectively, while sandy land, other land, and agricultural land reduced by 88.07%, 65.80%, and 46.70% from 1990 to 2019.

Table 4. Summary of land cover classes and change on Haitan Island, China.

Land Cover Classes	Area (km ²)				Change in Area (%)			
	1990	2000	2007	2019	1990–2000	2000–2007	2007–2019	1990–2019
Sandy land	14.30	6.66	1.07	4.89	−53.43	−83.85	354.90	−65.80
Built-up land	17.87	26.86	48.39	65.14	50.24	80.17	34.63	264.43
Cultivated land	69.74	60.14	46.69	37.17	−13.76	−22.36	−20.39	−46.70
Forest land	58.89	89.80	146.25	151.25	52.49	62.86	3.42	156.85
Other land	89.76	62.57	2.60	10.71	−30.29	−95.85	312.37	−88.07
Water	9.68	14.22	15.25	13.20	46.87	7.24	−13.43	36.36

The built-up land areas and forest land areas were continuously increasing over the whole period from 1990 to 2019, while cultivated land areas were gradually decreasing. Other land and sandy land areas showed a similar trend, reducing from 1990 to 2007, but increasing between 2007 and 2019 (Figure 4). In 1990, sandy land covered 14.30 km² of Haitan Island, while this dropped to 1.07 km² in 2007 and increased in 2019 (4.89 km²). The built-up land areas expanded by 8.98 km² between 1990 and 2000 and substantially grew by 21.53 km² and 16.76 km² between the second (2000–2007) and third (2007–2019) intervals, respectively. Water areas experienced an increase of 4.54 km² between 1990 and 2000 and 1.03 km² between 2000 and 2007 and decreased between 2007 and 2019 (2.05 km²). The cultivated land continuously declined by 9.60 km² between 1990 and 2000, 13.45 km² between

2000 and 2007, and 9.52 km² between 2007 and 2019. The other land areas showed a significant change between 1990 and 2019, with a decrease of 27.19 km² and 59.98 km² in the first and second intervals, and an increase of 8.11 km² in the third interval.

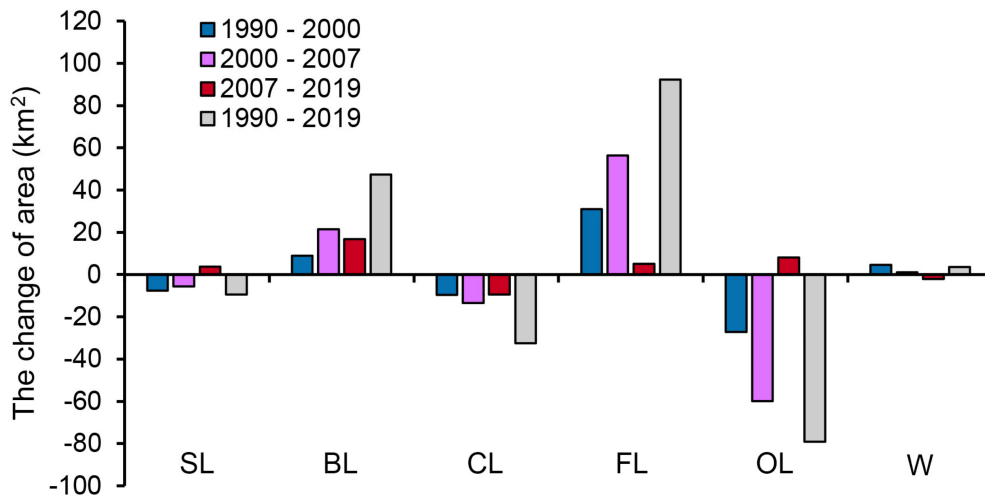


Figure 4. The change in the area of land cover classes in different time intervals: 1990–2000, 2000–2007, 2007–2019, and 1990–2019. SL = sandy land, BL = built-up land, CL = cultivated land, FL = forest land, OL = other land, W = water.

3.3. The Spatial Patterns of Land Cover Change

Figure 5 shows the transition of each land cover type during different intervals. In the periods between 1990–2000 and 2000–2007, the greatest transition was other land to forest land. Between 2007 and 2019, some of the forest land was transformed into other land, and most of them remained unchanged. For the whole period, the predominant land cover transitions were other land and cultivated land areas to forest land area.

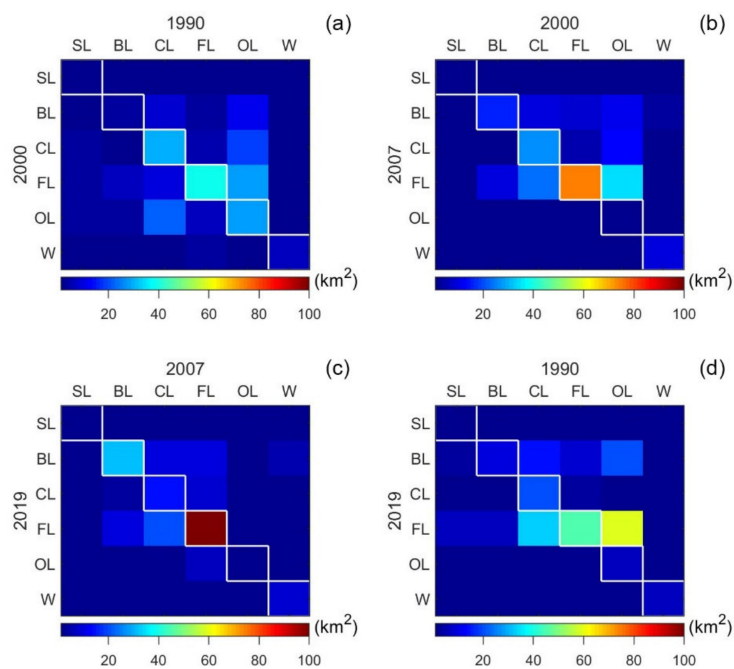


Figure 5. Conversion matrix of land use: (a) 1990–2000, (b) 2000–2007, (c) 2007–2019, and (d) 1990–2019. SL = sandy land, BL = built-up land, CL = cultivated land, FL = forest land, OL = other land, W = water.

Over the past 30 years, forest, cultivated land, and built-up land were the major changed land cover types. The spatial patterns of these land cover changes are shown in Figure 6a–f, which progressed as follows: Reforestation, cultivated land shrink, and built-up land expansion.

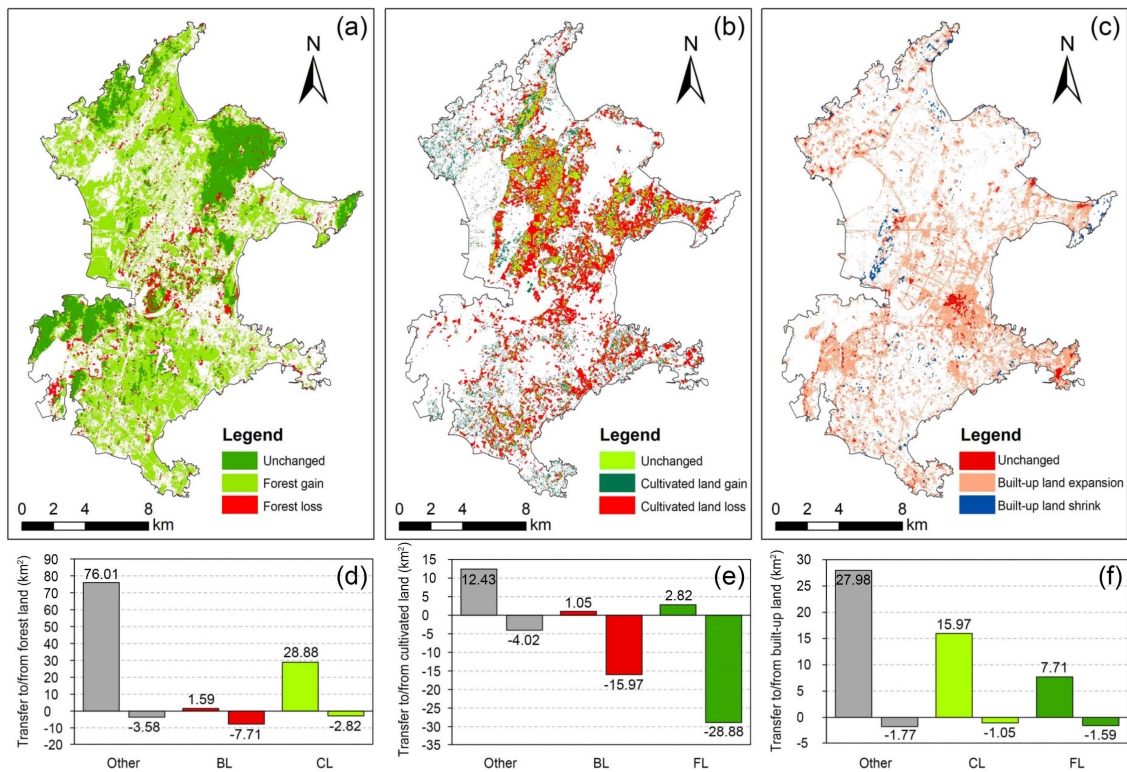


Figure 6. The main land cover types: (a) forest change, (b) cultivated land change, and (c) built-up land change loss and gain between 1990 and 2019 and their conversion. Transfer to/from (d) forest land, (e) cultivate land, and (f) built-up land. Other = sandy land, water, and other land; BL = built-up land, CL = cultivated land, FL = forest land.

The results of forest change analysis show 106.48 km² of forest gain and 14.11 km² of forest loss between 1990 and 2019 (Figure 6d). Forest gain area was transferred from cultivated land (28.88 km²), built-up land (1.59 km²), and other land cover types (76.01 km²), respectively. The area of forest gain is larger on the western than the eastern area of the Island. Forest loss area was transferred to cultivated land (2.82 km²), built-up land (7.71 km²), and other land cover types (3.58 km²), respectively. Cultivated land loss amounted to 48.87 km² on Haitan Island, with 41.64% (28.88 km²), 23.03% (15.97 km²), and 5.80% (4.02 km²) converted to forest, built-up land, and other land cover types, respectively. The most apparent reduction occurred in the middle of Haitan Island. A total of 51.66 km² of built-up land expanded from other land cover types (27.98 km²), cultivated land (15.97 km²), and forest land (7.71 km²). The most obvious built-up land expansion occurred in the middle of Haitan Island (e.g., Tancheng town). Meanwhile, in order to evaluate the influence of LULC changes, the maximum NDVI in the years of 1990, 2000, 2007, and 2019 was calculated (Figure 7). Comparing the maximum NDVI in a given year, more greenery and fragmentation of Haitan Island can be seen in 2019, which indicated that the vegetation increased and was accompanied by built-up land expansion.

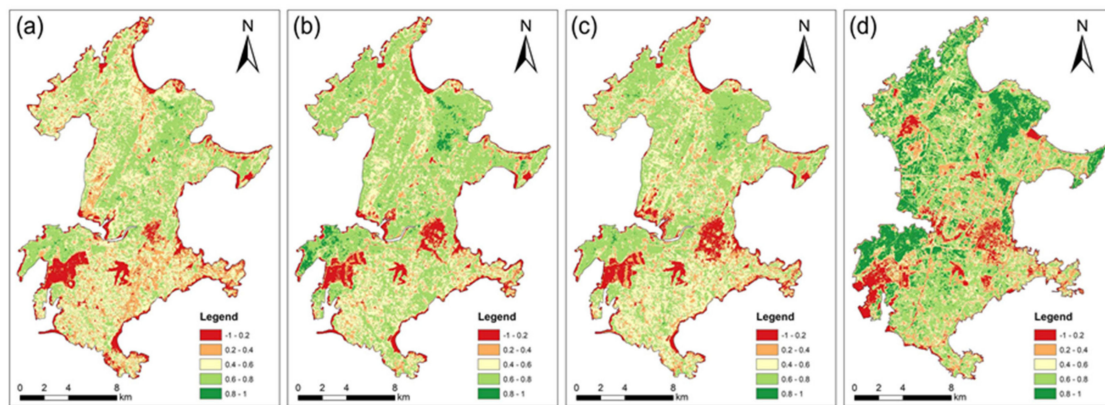


Figure 7. The maximum NDVI: (a) 1990, (b) 2000, (c) 2007, and (d) 2019 on Haitan Island.

4. Discussion

4.1. Land Cover Change from 1990 to 2019

The dominant land cover in 1990, covering 34.49% of the study area, was other land (89.76 km²), followed by 26.80% cultivated land (69.74 km²). In comparison, 53.57% of forest land and 23.07% of built-up land were the dominant land cover types in 2019. Similar to previous research [6], results of this study showed a continuous decline of cultivated land on Haitan Island, which was mostly converted to forest and built-up land (Figures 5 and 6). Other land and sandy land showed the same trend, which reduced from 1990 to 2000 and 2000 to 2007 but increased since 2007.

The spatial pattern was used to identify the major land cover types' change. The results showed that reforestation, cultivated land reduction, and built-up land expansion were the major land cover change processes on Haitan Island. The reforestation process was more evident on the western coast than the eastern coast, which implies a threat by the wind-related environment on the eastern coast.

4.2. Effects of Reforestation on Land Cover Change

The sandy lands are mainly located in the windward direction of each bay (e.g., Changjiang Bay, Haitan Bay, and Tannan Bay). The area of sandy land decreased by 13.22 km² between 1990 and 2007, and the reason can be explained by policy-making that aims at sand control on Haitan Island. Local forestry bureau, Fujian Academy of forestry, and other relevant institutions carried out reforestation projects in Pingtan County [27]. The coastal forests have an advantage in windbreak and sand fixation, which protects Haitan Island's ecosystems and the environment from wind damage. Nevertheless, in 2007–2019, the area of sandy land increased by 3.81 km². The fact may be explained by the possible conversion of other land use types into bare land because of the development process to support the tourism and built-up land development [38] and the construction of roads and wind power stations near the location of wind gaps. Massive construction reduces the windproof ability of shelter forests and forms new wind gaps, which push the development of sand [27].

Reforestation can contribute to local ecological restoration, coastal protection, and urban green space expansion [39]. In this study, forest land had experienced significant growth over the past three decades. The maximum NDVI showed Haitan Island was greener in 2019 than before (Figure 7), which indicated the effects of reforestation. Overall, forest change on Haitan Island reflects the ability of anthropogenic activities to transform natural landscapes. Although the pattern of forest change was discussed in this study, forest species and quality on Haitan Island remain unknown. According to incomplete statistics based on the forest survey data, black pine was the dominant tree species in Pingtan Island for wind prevention in the 1990s, but beach sheoak subsequently became the major tree species [27]. In addition, due to the continuous reforestation processes and in favor of the goal

of international tourism, varieties of tree species were cultivated on Haitan Island in recent years. Therefore, the change of forest species and quality on Haitan Island needs to be further studied.

4.3. Drivers of LULC Change

Reforestation and built-up expansion were accompanied by a decrease in cultivated land on Haitan Island. Results from this study showed that built-up expansion and cultivated land reduction were concentrated in the middle of the island. The reason for this phenomenon is related to government development policy [39]. According to the national development strategy, the layout planning of 'Comprehensive Pilot Zone' focused on the central and western plain regions' development [29]. Under the guideline of strategy, the cross-strait bridge was built in 2010 [39], which connects Pingtan Island and mainland China and boosts its development. Pingtan cross-strait, highway–railway bridge nears completion, and the high-speed rail will be open to traffic in the coming years. The station is located in Tancheng town, in the middle of the island. Those measures accelerate urban development of Pingtan Island. Likewise, the 'Grain for Green Project' contributed to cultivated land transfer to forest land. Similar projects have also greatly contributed to forest increase in other parts of China due to government policy making, for instance, Three North Protection Forest Project [25,40]. This program is successful in protecting the ecosystem and environment by afforestation based on the guideline of national strategy. Zhai et al. (2013) [41] discussed reforestation efforts and payments for ecosystem services' programs on tropical Hainan Island, where the Sloping Land Conversion Program (SLCP) increased tree cover on the island while losing diverse natural forests. Zhai et al. (2013) [41] discussed the limitations of using "forests" as a classification category in forest restoration programs because it includes both natural, native, and non-native forests. According to Xu (2011) [42], continued use of general category "forest" would further risk tropical natural forests and associated biodiversity. Economic subsidies to plant non-native monoculture-type forests (e.g., rubber plantations, etc.) would further place conversion pressure on natural forests [41]. Zhang et al. (2000) [43] conducted an econometric analysis of the causes of forest land use changes on Hainan Island and concluded that population growth was behind the decrease in natural forests. In addition, higher timber prices led to rain forest loss while increasing the area of plantation forests [43].

Besides the policy factor for land use transition, population and economic activity also have contributed to land cover change. According to the Fuzhou Statistical Yearbook [44], the urban population of Pingtan County was 94,500 people in 1990, which increased to 230,900 people in 2019. The population increased considerably in the town of Tancheng (County government location). The growing population results in the expansion of built-up land, such as road construction, industry, residential houses, and other changes. The GDP of Pingtan County was 46.03, 455.59, 772.94, and 4159.56 million USD in 1990, 2000, 2007, and 2019, respectively, which indicated rapid economic growth. In addition, another threat to sustainable development in Pingtan County is physical factors, particularly strong wind [23]. With further uncertainty factors arising in recent years, the balance between nature conservation and socio-economic development is necessary.

4.4. Advantages of Using GEE and Data Limitations

GEE provides an unprecedented opportunity to handle time-series images efficiently. Previous research reported combining NDVI, NDBI, and other indexes to improve classification accuracy [19,45]. For instance, Liu et al. (2020) [14] proposed to add the annual minimum built-up composites, texture features' usable image, and other indices to bands for image classification. Zurqani et al. (2019) [46] used NDVI, EVI, GRVI, MSAVI, and NDWI for classification in Greenville, South Carolina. In this study, NDVI, NDBI, MNDWI, and tasseled cap (brightness, greenness, wetness) were added to Landsat images and achieved satisfactory classification. For better accuracy of classification, it has not only high-resolution images (e.g., Sentinel datasets) but also supports HSV-based Pan-Sharpener algorithm for Landsat in GEE, which is helpful for classification. However, it is limited to processing post-classification [14] and lacks an interactive interface to modify the classification.

In addition, combining images from different time periods can improve the accuracy of classification. For instance, Figure 8 shows the Landsat image of Haitan Island in April 2020 and June 2020, respectively, where the increased pixel values from cultivated land are evident in the June image. Cultivated land can be identified accurately by evaluating both growing season and fallow season images. It is, however, challenging to acquire both the growing season and fallow season images in each of the study years due because there is often cloud coverage in the study area.

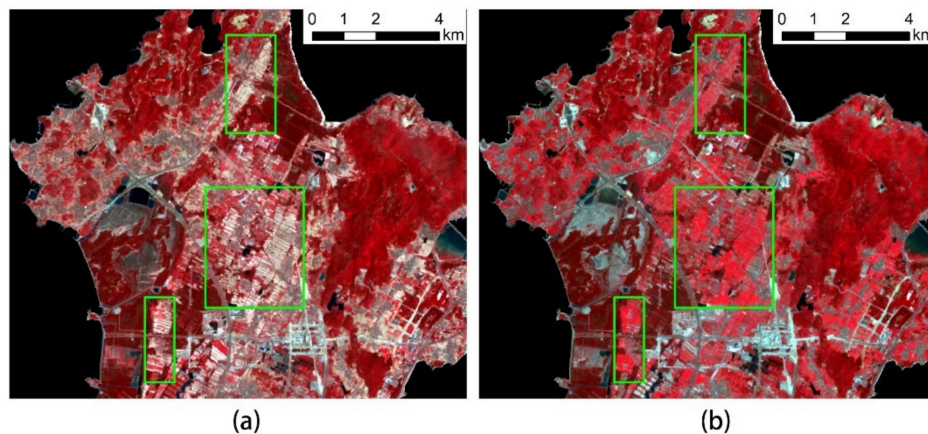


Figure 8. Cultivated land in the north and west of Haitan Island: (a) fallow season, Landsat image obtained in April 2020, (b) growing season, Landsat image obtained in June 2020 (subset of Landsat 8 OLI, shown with band 5, 4, and 3 in red, green, and blue).

For long-time temporal observations, Landsat datasets are the only option for tracking the continuous land cover change from the 1990s. In this study, the maximum NDVI composition was selected from all the available images in a given year to evaluate the influence of LULC changes. However, although GEE provides algorithms to combine multiple images for re-assembling a cloud-free image, Landsat series datasets and other optical satellite data always contain more cloud cover in the coastal area. Some NDVI values might not represent the maximum NDVI values due to the limited images in a given year because of the influence caused by haze and clouds in the image [30]. Therefore, it is more challenging to achieve long-term observation and evaluation in coastal areas [24].

5. Conclusions

Satellite classification has most often been used to document environmental losses in the face of urbanization. This study is unique because it provides an efficient methodology for temporal land use classification and forest detection for island environments while showing combined reforestation and urbanization over time. Google Earth Engine was used to classify Landsat satellite images to track land cover change for Haitan Island from 1990 to 2019. A multi-temporal, remote sensing database was instantly available via GEE's data library and cloud computing environment, which provides access to high-throughput computing at no cost for noncommercial uses. Image analysis in GEE showed that Haitan Island experienced a dramatic land cover change from 1990 to 2019. User and producer accuracies were consistently higher than 80% for the classified images. The overall accuracy and Kappa coefficient values ranged from 88.43% to 91.08% and 0.86 to 0.90, respectively. The results showed that over the past 30 years (1990–2019) Haitan Island has experienced an increase in forest land (30.94%) and built-up land (30.70%) and a decrease in cultivated land (13.63%) and sandy land (3.76%) in the study area. In general, LULC experienced a significant change, which may be due to socio-economic factors (e.g., population growth, anthropogenic activities), policy decision making (fast-growing economy and reforestation), and physical factors. The increases in the forest area show that the reforestation efforts have been successful even though there has been increased urbanization. These reforestation efforts are particularly important in this island environment where the trees serve as sand-control and

windbreaks. Continuous monitoring of island environments and sustainability, in the face of climate change and population pressures, using GEE and satellite image classification helps regionalized land-use policy-making and represents an important example for other island environments that may face similar issues. Future analysis can be enhanced by using science-based "forests" category, which includes differentiating by the type of forests (e.g., native, non-native, etc.) and economic analysis of drivers in changes between native and non-native forests.

Author Contributions: Conceptualization, methodology and software, L.L. and Z.H.; investigation, K.Y. and L.Y.; data curation, writing—original draft preparation and visualization, L.L.; writing—review and editing, C.J.P. and E.A.M.; supervision, project administration, J.L.; funding acquisition, J.L. and K.Y. All authors have read and agreed to the published version of the manuscript.

Funding: This research was funded by National Major Science and Technology Projects of China, grant number 2018YFD060010304, Fujian Provincial Department of Science and Technology, grant number 2019N5012, and the scholarship program of China Scholarship Council, grant number 201908350124.

Acknowledgments: We wish to thank the anonymous reviewers and editors for their professional comments and suggestions. We also want to thank Eshetu Shifaw and Yung-Chih Su for technical support in Figure 5.

Conflicts of Interest: The authors declare no conflict of interest.

Glossary

EVI	Enhanced Vegetation Index
GEE	Google Earth Engine
GRVI	Green-Red Vegetation Index
HSV	Hue-Saturation-Value
LULC	Land use and land cover
MSAVI	Modified Soil-adjusted Vegetation Index
MNDWI	Modified Normalized Difference Water Index
MODIS	Moderate Resolution Imaging Spectroradiometer
NIR	Near-infrared
NDVI	Normalized Difference Vegetation Index
NDBI	Normalized Difference Built-up Index
NDWI	Normalized Difference Water Index
OLI	Operational Land Imager
RGB	Red, green, blue bands
SWIR	Short-wave infrared

References

1. Kueffer, C.; Kinney, K. What is the importance of islands to environmental conservation? *Environ. Conserv.* **2017**, *44*, 311–322. [[CrossRef](#)]
2. Kuemmerle, T.; Levers, C.; Erb, K.; Estel, S.; Jepsen, M.R.; Müller, D.; Plutzer, C.; Stürck, J.; Verkerk, P.J.; Verburg, P.H.; et al. Hotspots of land use change in Europe. *Environ. Res. Lett.* **2016**, *6*, 64020. [[CrossRef](#)]
3. Montoya-Tangarife, C.; de la Barrera, F.; Salazar, A.; Inostroza, L. Monitoring the effects of land cover change on the supply of ecosystem services in an urban region: A study of Santiago-Valparaíso, Chile. *PLoS ONE* **2017**, *12*, e188117. [[CrossRef](#)] [[PubMed](#)]
4. Abdullah, A.Y.M.; Masrur, A.; Adnan, M.S.G.; Baky, M.A.A.; Hassan, Q.K.; Dewan, A. spatio-temporal patterns of land use/land cover change in the heterogeneous coastal region of Bangladesh between 1990 and 2017. *Remote Sens.* **2019**, *11*, 790. [[CrossRef](#)]
5. Fonseka, H.P.U.; Zhang, H.; Sun, Y.; Su, H.; Lin, H.; Lin, Y. Urbanization and its impacts on land surface temperature in Colombo metropolitan area, Sri Lanka, from 1988 to 2016. *Remote Sens.* **2019**, *11*, 957. [[CrossRef](#)]
6. Shifaw, E.; Sha, J.; Li, X.; Bao, Z.; Legass, A.; Belete, M.; Ji, J.; Su, Y.; Addis, A.K. Farmland dynamics in Pingtan, China: Understanding its transition, landscape structure and driving factors. *Environ. Earth Sci.* **2019**, *78*. [[CrossRef](#)]
7. Viana, C.M.; Girão, I.; Rocha, J. Long-term satellite image time-series for land use/land cover change detection using refined open source data in a rural region. *Remote Sens.* **2019**, *11*, 1104. [[CrossRef](#)]

8. Wang, L.; Diao, C.; Xian, G.; Yin, D.; Lu, Y.; Zou, S.; Erickson, T.A. A summary of the special issue on remote sensing of land change science with Google Earth Engine. *Remote Sens. Environ.* **2020**, *248*, 112002. [CrossRef]
9. Lee, J.S.H.; Wich, S.; Widayati, A.; Koh, L.P. Detecting industrial oil palm plantations on Landsat images with Google Earth Engine. *Remote Sens. Appl. Soc. Environ.* **2016**, *4*, 219–224. [CrossRef]
10. Gorelick, N.; Hancher, M.; Dixon, M.; Ilyushchenko, S.; Thau, D.; Moore, R. Google Earth Engine: Planetary-scale geospatial analysis for everyone. *Remote Sens. Environ.* **2017**, *202*, 18–27. [CrossRef]
11. Hansen, M.C.; Potapov, P.V.; Moore, R.; Hancher, M.; Turubanova, S.A.; Tyukavina, A.; Thau, D.; Stehman, S.V.; Goetz, S.J.; Loveland, T.R.; et al. High-resolution global maps of 21st-century forest cover change. *Science* **2013**, *342*, 850–853. [CrossRef] [PubMed]
12. Moore, R.; Hansen, M. Google Earth Engine: A New Cloud-Computing Platform for Global-Scale Earth Observation Data and Analysis. Available online: <http://adsabs.harvard.edu/abs/2011AGUFMIN43C.02M> (accessed on 1 October 2020).
13. Joshi, A.R.; Dinerstein, E.; Wikramanayake, E.; Anderson, M.L.; Olson, D.; Jones, B.S.; Seidensticker, J.; Lumpkin, S.; Hansen, M.C.; Sizer, N.C.; et al. Tracking changes and preventing loss in critical tiger habitat. *Sci. Adv.* **2016**, *2*, e1501675. [CrossRef] [PubMed]
14. Liu, D.; Chen, N.; Zhang, X.; Wang, C.; Du, W. Annual large-scale urban land mapping based on Landsat time series in Google Earth Engine and OpenStreetMap data: A case study in the middle Yangtze River basin. *ISPRS J. Photogramm.* **2020**, *159*, 337–351. [CrossRef]
15. Liu, X.; Hu, G.; Chen, Y.; Li, X.; Xu, X.; Li, S.; Pei, F.; Wang, S. High-resolution multi-temporal mapping of global urban land using Landsat images based on the Google Earth Engine Platform. *Remote Sens. Environ.* **2018**, *209*, 227–239. [CrossRef]
16. Benz, S.A.; Bayer, P.; Blum, P. Identifying anthropogenic anomalies in air, surface, and groundwater temperatures in Germany. *Sci. Total Environ.* **2017**, *584–585*, 145–153. [CrossRef]
17. Tamiminia, H.; Salehi, B.; Mahdianpari, M.; Quackenbush, L.; Adeli, S.; Brisco, B. Google Earth Engine for geo-big data applications: A meta-analysis and systematic review. *ISPRS J. Photogramm.* **2020**, *164*, 152–170. [CrossRef]
18. Zurqani, H.A.; Post, C.J.; Mikhailova, E.A.; Schlautman, M.A.; Sharp, J.L. Geospatial analysis of land use change in the Savannah River Basin using Google Earth Engine. *Int. J. Appl. Earth Obs.* **2018**, *69*, 175–185. [CrossRef]
19. Huang, H.; Chen, Y.; Clinton, N.; Wang, J.; Wang, X.; Liu, C.; Gong, P.; Yang, J.; Bai, Y.; Zheng, Y.; et al. Mapping major land cover dynamics in Beijing using all Landsat images in Google Earth Engine. *Remote Sens. Environ.* **2017**, *202*, 166–176. [CrossRef]
20. Meng, Y.; Liu, X.; Wu, L.; Liu, M.; Zhang, B.; Zhao, S. Spatio-temporal variation indicators for landscape structure dynamics monitoring using dense normalized difference vegetation index time series. *Ecol. Indic.* **2019**, *107*, 105607. [CrossRef]
21. Venter, Z.S.; Scott, S.L.; Desmet, P.G.; Hoffman, M.T. Application of Landsat-derived vegetation trends over South Africa: Potential for monitoring land degradation and restoration. *Ecol. Indic.* **2020**, *113*, 106206. [CrossRef]
22. Li, Q.; Huang, J.; Wang, C.; Lin, H.; Zhang, J.; Jiang, J.; Wang, B. Land development suitability evaluation of Pingtan Island based on scenario analysis and landscape ecological quality evaluation. *Sustainability* **2017**, *9*, 1292. [CrossRef]
23. Zheng, S.; Yu, B. Landsenses pattern design to mitigate gale conditions in the coastal city—a case study of Pingtan, China. *Int. J. Sustain. Dev. World Ecol.* **2016**, *24*, 352–361. [CrossRef]
24. Gutiérrez Rodríguez, L.; Hogarth, N.J.; Zhou, W.; Xie, C.; Zhang, K.; Putzel, L. China’s conversion of cropland to forest program: A systematic review of the environmental and socio-economic effects. *Environ. Evid.* **2016**, *5*, 21. [CrossRef]
25. Ahrends, A.; Hollingsworth, P.M.; Beckschäfer, P.; Chen, H.; Zomer, R.J.; Zhang, L.; Wang, M.; Xu, J. China’s fight to halt tree cover loss. *Proc. R. Soc. B* **2017**, *1854*, 20162559. [CrossRef]
26. Free Trade Zone Included 43 Square Kilometers of Pingtan Area. Available online: www.pingtan.gov.cn/jhtml/ct/ct_2925_41940 (accessed on 15 July 2020).
27. Yue, X. Optimization on the Protection Forest of Casuarina Equisetifolia in the Southeast Coast of China—a Case Study in Pingtan County, Fujian Province. Master’s Thesis, Fujian Agriculture and Forestry University, Fujian, China, 2010.

28. Peng, X.; Ding, F.; Wu, W.; Zhang, X. Remote sensing monitoring of wind-preventing and sand-fixing effects of coastal protection forests: A case study in Haitan Island, Fujian, China. In Proceedings of the Third International Workshop on Earth Observation and Remote Sensing Applications (EORSA), Changsha, China, 11–14 June 2014; pp. 57–61. [\[CrossRef\]](#)
29. Shifaw, E.; Sha, J.; Li, X.; Bao, Z.; Zhou, Z. An insight into land-cover changes and their impacts on ecosystem services before and after the implementation of a comprehensive experimental zone plan in Pingtan Island, China. *Land Use Policy* **2019**, *82*, 631–642. [\[CrossRef\]](#)
30. Huang, C.; Wylie, B.; Yang, L.; Homer, C.; Zylstra, G. Derivation of a tasselled cap transformation based on Landsat 7 at-satellite reflectance. *Int. J. Remote Sens.* **2002**, *23*, 1741–1748. [\[CrossRef\]](#)
31. Baig, M.H.A.; Zhang, L.; Shuai, T.; Tong, Q. Derivation of a tasselled cap transformation based on Landsat 8 at-satellite reflectance. *Remote Sens. Lett.* **2014**, *5*, 423–431. [\[CrossRef\]](#)
32. Li, X.; Zhou, Y.; Zhu, Z.; Liang, L.; Yu, B.; Cao, W. Mapping annual urban dynamics (1985–2015) using time series of Landsat data. *Remote Sens. Environ.* **2018**, *216*, 674–683. [\[CrossRef\]](#)
33. Tong, X.; Brandt, M.; Hiernaux, P.; Herrmann, S.; Rasmussen, L.V.; Rasmussen, K.; Tian, F.; Tagesson, T.; Zhang, W.; Fensholt, R. The forgotten land use class: Mapping of fallow fields across the Sahel using Sentinel-2. *Remote Sens. Environ.* **2020**, *239*, 111598. [\[CrossRef\]](#)
34. Pelletier, C.; Valero, S.; Inglada, J.; Champion, N.; Dedieu, G. Assessing the robustness of Random Forests to map land cover with high resolution satellite image time series over large areas. *Remote Sens. Environ.* **2016**, *187*, 156–168. [\[CrossRef\]](#)
35. Ge, Y.; Hu, S.; Ren, Z.; Jia, Y.; Wang, J.; Liu, M.; Zhang, D.; Zhao, W.; Luo, Y.; Fu, Y.; et al. Mapping annual land use changes in China’s poverty-stricken areas from 2013 to 2018. *Remote Sens. Environ.* **2019**, *232*, 111285. [\[CrossRef\]](#)
36. Deus, D. Integration of ALOS PALSAR and Landsat data for land cover and forest mapping in Northern Tanzania. *Land* **2016**, *5*, 43. [\[CrossRef\]](#)
37. Zhu, Z.; Woodcock, C.E.; Olofsson, P. Continuous monitoring of forest disturbance using all available Landsat imagery. *Remote Sens. Environ.* **2012**, *122*, 75–91. [\[CrossRef\]](#)
38. Yu, F.; Cai, F.; Ren, J.; Liu, J. Island beach management strategy in China with different urbanization level—Take examples of Xiamen Island and Pingtan Island. *Ocean Coast. Manag.* **2016**, *130*, 328–339. [\[CrossRef\]](#)
39. Shifaw, E.; Sha, J.; Li, X. Detection of spatiotemporal dynamics of land cover and its drivers using remote sensing and landscape metrics (Pingtan Island, China). *Environ. Dev. Sustain.* **2018**, *22*, 1269–1298. [\[CrossRef\]](#)
40. Zhang, L.; Schwärzel, K. China’s land resources dilemma: Problems, outcomes, and options for sustainable land restoration. *Sustainability* **2017**, *9*, 2362. [\[CrossRef\]](#)
41. Zhai, D.; Xu, J.; Dai, Z.; Cannon, C.H.; Grumbine, R.E. Increasing tree cover while losing diverse natural forests in tropical Hainan, China. *Reg. Environ. Chang.* **2014**, *14*, 611–621. [\[CrossRef\]](#)
42. Xu, J. China’s new forests aren’t as green as they seem. *Nature* **2011**, *477*, 371. [\[CrossRef\]](#)
43. Zhang, Y.Q.; Uusivuori, J.; Kuuluvainen, J. Econometric analysis of the causes of forest land use changes in Hainan, China. *Can. J. For. Res.* **2000**, *30*, 1913–1921. [\[CrossRef\]](#)
44. Fuzhou Statistical Yearbook. Available online: <http://61.186.207.3:7300/Yearbook/Single/N2019010169> (accessed on 15 July 2020).
45. Grogan, K.; Pflugmacher, D.; Hostert, P.; Kennedy, R.; Fensholt, R. Cross-border forest disturbance and the role of natural rubber in mainland Southeast Asia using annual Landsat time series. *Remote Sens. Environ.* **2015**, *169*, 438–453. [\[CrossRef\]](#)
46. Zurqani, H.A.; Post, C.J.; Mikhailova, E.A.; Allen, J.S. Mapping urbanization trends in a forested landscape using Google Earth Engine. *Remote Sens. Earth Syst. Sci.* **2019**, *2*, 173–182. [\[CrossRef\]](#)

Publisher’s Note: MDPI stays neutral with regard to jurisdictional claims in published maps and institutional affiliations.



© 2020 by the authors. Licensee MDPI, Basel, Switzerland. This article is an open access article distributed under the terms and conditions of the Creative Commons Attribution (CC BY) license (<http://creativecommons.org/licenses/by/4.0/>).